

PAPER • OPEN ACCESS

## Effect of inclusion of pitch-angle dependence on a simplified model of RF deposition in tokamak plasma

To cite this article: D M A Taylor *et al* 2022 *Plasma Phys. Control. Fusion* **64** 055015

View the [article online](#) for updates and enhancements.

### You may also like

- [MHD spectroscopy of JET plasmas with pellets via Alfvén eigenmodes](#)  
S.E. Sharapov, H.J.C. Oliver, B.N. Breizman *et al.*
- [Analysis of resonant fast ion distributions during combined ICRF and NBI heating with transients using neutron emission spectroscopy](#)  
C. Hellesen, M. Mantsinen, S. Conroy *et al.*
- [Modelling third harmonic ion cyclotron acceleration of deuterium beams for JET fusion product studies experiments](#)  
M. Schneider, T. Johnson, R. Dumont *et al.*





**IOP | ebooks™**

Bringing together innovative digital publishing with leading authors from the global scientific community.

Start exploring the collection—download the first chapter of every title for free.

# Effect of inclusion of pitch-angle dependence on a simplified model of RF deposition in tokamak plasma

D M A Taylor<sup>1,\*</sup> , M J Mantsinen<sup>2,3</sup>, D Gallart<sup>2</sup> , J Manyer<sup>2</sup>, P Sirén<sup>1</sup>  
and JET Contributors<sup>4</sup>

<sup>1</sup> United Kingdom Atomic Energy Authority, Culham Centre for Fusion Energy, Culham Science Centre, Abingdon, Oxon OX14 3DB, United Kingdom

<sup>2</sup> Barcelona Supercomputing Centre (BSC), Barcelona, Spain

<sup>3</sup> ICREA, Barcelona, Spain

E-mail: [david.taylor@ukaea.uk](mailto:david.taylor@ukaea.uk)

Received 21 December 2021, revised 25 February 2022

Accepted for publication 16 March 2022

Published 11 April 2022



CrossMark

## Abstract

Using the PION ICRH modelling code and comparisons against JET tokamak experiments, the effect of including pitch angle dependence within the RF diffusion operator on the fast ion particle distribution functions is quantified. It is found to be of greatest importance in cases of higher harmonic heating and lower heating ion mass, resulting in faster drop-off of the distribution's high energy tail. We see differences of several orders of magnitude in the high-energy range and significant non-linear alterations by several tens of percent to ion species power partition. ITER scenario operational parameters are also considered, and this improved treatment is shown to benefit anticipated ITER scenarios with second harmonic hydrogen heating, according to our predictions. PION's combination of benchmarked simplified wave physics and Fokker-Planck treatment offers modelling advantages. Since including the pitch angle dependence in the RF diffusion operator has not led to a significant increase in the required computing time when modelling different ICRF schemes in JET discharges, it has been made available within the production code.

Keywords: tokamak, ICRF, PION, fast ions, neutron spectroscopy, JET, ITER

<sup>4</sup> See the author list of 'Overview of JET results for optimising ITER operation' by J Mailloux *et al* to be published in Nuclear Fusion Special issue: Overview and Summary Papers from the 28th Fusion Energy Conference (Nice, France, 10–15 May 2021).

\* Author to whom any correspondence should be addressed.



Original content from this work may be used under the terms of the [Creative Commons Attribution 4.0 licence](https://creativecommons.org/licenses/by/4.0/). Any further distribution of this work must maintain attribution to the author(s) and the title of the work, journal citation and DOI.

## 1. Introduction

Radio frequency auxiliary heating of tokamak plasma in the ion cyclotron frequency range is now a common technique for a variety of plasma ion compositions, used on many present and planned toroidal plasma devices [1–3].

PION is a well-established computing tool that evolves the time-evolution of ICRH power absorption and the distribution functions of the resonant ions in a self-consistent way [4, 5]. Extensively validated against experimental data on JET [5–13], AUG [14–17], DIII-D [18], and WEST (formerly Tore Supra) [19, 20] for many minority and majority heating schemes, its models use simplified physics, making it a versatile and relatively fast solver suitable for prompt analysis. This speed sees it implemented as part of the automated data processing chain at JET (including an intershot version). It has been installed in the ITER Integrated Modelling and Analysis Suite, enabling integrated predictive modelling of ITER plasmas [21].

ICRH modelling is relatively complex, due to the need to solve Fokker-Planck and wave equations in a self-consistent way. PION's principal physics simplifications are twofold: firstly, the wave power deposition is taken to be a superposition of strong and weak absorption limit cases; secondly, the Fokker-Planck equation is modelled as a function of flux surface, scalar velocity, and time only.

We consider here comparisons of PION fast ion distribution functions with diagnostic results from the 2.5 MeV TOFOR neutron spectrometer and the High Energy Neutral Particle Analyser, revisiting PION modelling for pulses previously published by Salmi [11] and Schneider [22].

This paper presents the effect of including pitch angle dependence within the RF diffusion operator calculation. This contrasts with earlier calculations, made using pitch angle averaging. The implementation of this feature in production code is new, following the proof of principle demonstration given in [23] using third harmonic heating of D. Different ICRH codes treat the pitch angle in other ways, and listing them is beyond the scope of this paper. Such codes have been listed and reviewed thoroughly elsewhere [24].

In this work, we expand the study in [23] in the following ways: we quantify the differences between the old and new treatment in terms of changes in the ICRF diffusion coefficient as well as the simulated distribution function and power partitioning, expand the study for other heating schemes to validate the model, make it available for routine ICRF modelling use, and discuss its potential effects for ITER plasmas with ICRF heating. The changes implemented have only small effect in most modelling cases, of order 5% for global quantities. Runtime is increased by factors of up to approximately two for relevant cases. For example, in the common situation of modelling a fundamental resonance, little change is expected or observed. However, there are modelling cases where we can better match observations for some JET experimental regimes. We note the cases of second harmonic hydrogen heating and third harmonic deuterium heating, where the higher harmonic brings the minimum in the RF diffusion coefficient down to an energy value whose particle distribution is experimentally

measurable. Physically, this minimum expresses the energy value at which resonant Larmor radius accelerations and decelerations cancel [6], as derived in Kennel-Engelmann theory [25]. In general, higher harmonic heating is due to finite Larmor radius (FLR) effects, where ions experience both acceleration and deceleration around their orbits, and on average acceleration occurs if the particle distribution has a negative slope in velocity. We also note significant changes to the power absorption of heated ion species due to the changed diffusion coefficient.

To illustrate these tendencies, figure 1 shows the RF diffusion coefficient  $D_{\text{RF}}^N(v)$  with  $v$  assumed to be entirely perpendicular, resonant frequency held constant, and scaled to display values around unity. Under these conditions, the expression for the diffusion coefficient takes the simplified form shown in equation (1), as given in [6]

$$D_{\text{RF}}^N \propto \left| E_+ J_{n-1} \left( \frac{k_{\perp} v}{\omega_c} \right) + E_- J_{n+1} \left( \frac{k_{\perp} v}{\omega_c} \right) \right|^2. \quad (1)$$

Here  $J_n$  is a Bessel function of the first kind of order  $n$ ,  $N$  is the toroidal mode number,  $n$  is the ion cyclotron harmonic,  $f_{\text{ICRH}}$  is the frequency of the launched wave,  $E_+$  and  $E_-$  are respectively the left and right hand electric field components,  $\omega_c$  is the ion cyclotron frequency  $\frac{qB}{m}$  (with  $q$  the ionic charge,  $B$  the magnetic field, and  $m$  the ionic mass),  $k$  is the wavenumber,  $v$  the velocity, and the subscript  $\perp$  denotes the component of a quantity that is perpendicular to the magnetic field. Toroidal mode dependencies are found within the quantities held constant and are not explicit in this expression. Physically, the RF diffusion coefficient is proportional to the kick in energy given to the perpendicular velocity [26], and its tail corresponds to high energy absorption.

Figure 1(a) shows the functional dependence on harmonic number, which enters only in the Bessel function order. In consequence, there is marked similarity between the dependence of Bessel functions on order and this dependence on harmonic number. We observe the behaviour in the limit of zero velocity, where the presence of a  $J_0$  component in the fundamental heating expression implies substantial heating at low energies that is not present for higher harmonic heating, as shown in figure 1(a). We also observe the decreasing energy value of the function minimum as harmonic number increases to a value of 3, a characteristic not easily analytically provable, but one readily numerically demonstrated for a range of  $E_+/E_-$  exceeding experimental reality. This decrease of minimum position points to the increased importance of the method given here in second and third harmonic heating schemes.

Figure 1(b) shows the functional dependence on ion mass, which enters in the dependency on cyclotron frequency and the scaling from velocity to kinetic energy. The effect is of a linear stretching in energy; the energy position of the minimum is at twice the value for deuterium as for hydrogen, and three times for tritium.

The planned list of operational scenarios for ITER contains several that use second harmonic heating, and will also include

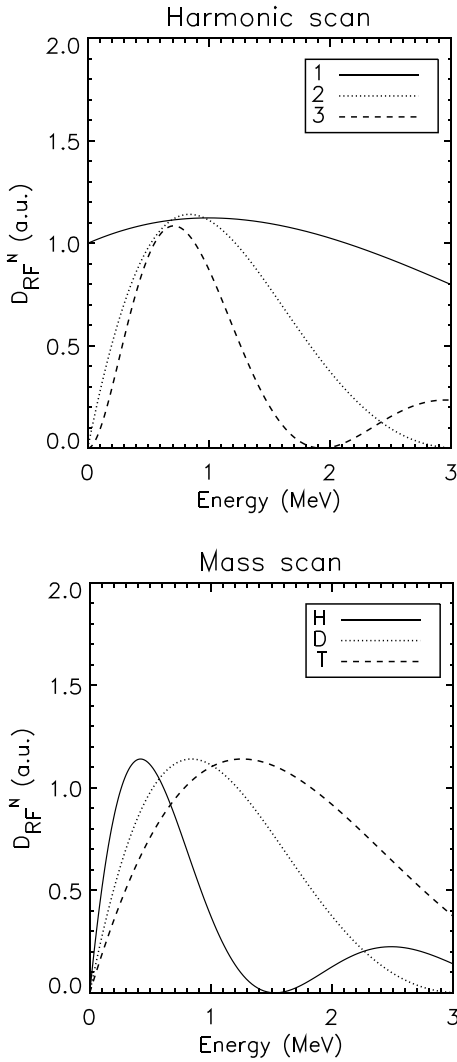


**Figure 1.** Variation of RF diffusion coefficient  $D_{RF}^N$  with energy for (a) harmonic number  $n$  with deuterium heating, and (b) ion mass with second harmonic heating. Parameters:  $k_{\perp} = 56.6 \text{ m}^{-1}$ ,  $\frac{E_{+}}{E_{-}} = 0.43$ ,  $f_{ICRH} = \frac{n\omega_c}{2\pi} = 51.5 \text{ MHz}$ .

plasmas with different ion isotope masses. So we see a natural relevance of this work to the experiments that will employ these scenarios, for which we expect the distribution function tail shape to be of importance.

In this paper, we will present firstly the necessary theoretical background, continue by comparing results, and conclude with some general remarks.

## 2. Theoretical background

### 2.1. PION overview

PION [4, 5] is a time-dependent code that models the deposition of ICRH power into tokamak plasma. Its attractiveness as a modelling tool lies in its tested simplifications of the full wave problem, allowing it to return results relatively rapidly for the full duration of a plasma discharge.

At each time step, it iterates two tasks. First, it calculates the power deposition. This is done by Fourier decomposition into individual toroidal modes. The power coupled to each mode is calculated according to the model described in [6], which was partly obtained by comparison with results from the full wave code LION [27, 28]. This model takes the deposited power as the superposition of weak and strong absorptions, partitioned as a function of the single pass absorption coefficient across the midplane [4]. The power lost to mode conversion is removed from the coupled power by using the Buden formula [29] to treat it as resonance absorption in a planar geometry.

Having modelled the deposition, PION then uses a one-dimensional Fokker-Planck equation to time-evolve the ion distribution function  $f(v)$ , calculating the power partition between heated species. The dielectric tensor components are updated with the output of this second part of the algorithm loop, and then fed back into the start of the loop process.

### 2.2. General theory background

For completeness we give the full three-dimensional description, then restrict to the used model.

We start from the general form of an orbit-averaged Fokker-Planck equation [30], equation (2):

$$\frac{\partial f}{\partial t} = \langle C(f) \rangle + \langle Q(f) \rangle \quad (2)$$

where  $\langle \rangle$  denotes an average over the drift orbit,  $t$  is time,  $f$  is a particle distribution function,  $C$  is a collision operator, and  $Q$  is a quasi-linear diffusion operator describing ICRH wave-particle interaction. When we average over orbits, the second term becomes

$$\langle Q(f) \rangle = \sum_N L_N (D_{RF}^N L_N f) \quad (3)$$

where  $L_N$  is a co-ordinate transformation operator expressed in terms of a set of invariants. Here again  $N$  is the toroidal wavenumber, and  $D_{RF}^N$  is the diffusion coefficient for that  $N$ .

Under orbit averaging, this description is three-dimensional, requiring three invariants to relate  $Q$  to  $D_{RF}$ . Following [31] and [5], we use the set  $(E, \Lambda, P_{\varphi})$ , where  $E$  is the ion energy,  $\Lambda = v_{\perp}^2 B_0 / v^2 B$ , and  $P_{\varphi}$  is the toroidal ion angular momentum  $mRv_{\phi} + Ze\psi_p$ . Here  $v$  is the ion velocity, the subscripts  $\phi$  and  $\perp$  denote respectively the components of a quantity that are toroidal and perpendicular to the magnetic field  $B$ ,  $B_0$  is the axial magnetic field,  $m$  is the ion mass,  $R$  is the major radius,  $Ze$  is the ion charge, and  $\psi_p$  is the poloidal magnetic flux. This permits the representation

$$L_N = \frac{\partial}{\partial E} + \frac{n\omega_{c0} - \Lambda\omega}{\omega E} \frac{\partial}{\partial \Lambda} + \frac{N}{\omega} \frac{\partial}{\partial P_{\varphi}} \quad (4)$$

with the diffusion coefficient  $D_{RF}^N$  taking the form [4]

$$D_{\text{RF}}^N = \frac{1}{4\omega^2} \sum_{\text{R}} \frac{(Ze)^2}{|n\dot{\omega}_{\text{cR}}|} v_{\perp\text{R}}^2 \left| E_+ J_{n-1} \left( \frac{k_{\perp} v_{\perp\text{R}}}{\omega_{\text{cR}}} \right) + E_- J_{n+1} \left( \frac{k_{\perp} v_{\perp\text{R}}}{\omega_{\text{cR}}} \right) \right|^2 \quad (5)$$

where the subscript R denotes points where the wave frequency matches the Doppler-shifted ion cyclotron frequency or its harmonic, which we refer to as ‘resonance points’. As before,  $n$  is the ion cyclotron harmonic,  $\omega$  is the frequency of the launched wave,  $E_+$  and  $E_-$  are respectively the left and right hand electric field components,  $\omega_{\text{c0}}$  is the ion cyclotron frequency at the magnetic axis,  $\omega_{\text{cR}}$  is the ion cyclotron frequency at the resonance point, and  $k$  is the wavenumber.

### 2.3. Development

Under PION’s formalism, which follows [32], the Fokker-Planck equation becomes (working in the small banana width limit  $|mRv_{\phi}| \ll Ze\psi_{\text{p}}$ ):

$$\frac{\partial F(v,t)}{\partial t} = \frac{1}{v^2} \frac{\partial}{\partial v} \left[ -\alpha v^2 F(v,t) + \frac{1}{2} \frac{\partial}{\partial v} (\beta v^2 F(v,t)) \right] + \frac{1}{v^2} \frac{\partial}{\partial v} \left[ v^2 D_{\text{RF}} \frac{\partial F(v,t)}{\partial v} \right] \quad (6)$$

where  $\alpha$  and  $\beta$  are parameters arising from the model that describes the collisional term [33], and  $F$  is a pitch angle averaged distribution function that is a function of scalar velocity and time only.

The second right hand side term of equation (6) details how the coefficient  $D_{\text{RF}}$  enters the model. Following [32], PION has modelled  $D_{\text{RF}}$  in pitch angle averaged fashion. This is a good assumption for the commonly-modelled case of fundamental heating, but less good for higher harmonic heating, due to the presence in expressions for  $D_{\text{RF}}$  of Bessel functions and their dependence on the harmonic number and ion mass.

In this paper we present the results of modelling  $D_{\text{RF}}$  with a resolved pitch angle. As we are working at a single time point, we now drop the time dimension in our notation. Following [23], we use the ansatz

$$F_{\mu}(v,\mu) = F(v) \frac{e^{-\left(\frac{\mu}{\Delta\mu(v)}\right)^2}}{\sqrt{\pi} \Delta\mu(v) \operatorname{erf}\left(\frac{1}{\Delta\mu(v)}\right)}. \quad (7)$$

Collisional pitch angle scattering is diffusive (i.e. entropy-increasing), and so a Gaussian makes a suitable approximation for this distribution [34].

Here erf is the Gaussian error function,  $F(v)$  is the pitch angle averaged distribution function,  $F_{\mu}(v,\mu)$  is the pitch angle resolved distribution function,  $\mu = v_{\parallel}/v$  is the cosine of the pitch angle of the ion relative to the background magnetic field, and the width of the exponential  $\Delta\mu(v)$  characterises the dependence of the distribution on the pitch angle. The valid range of the distribution is bounded in  $\mu$  by  $\pm 1$ , with the integral of the distributed function over this range being  $\int_{-1}^1 F_{\mu}(v,\mu) d\mu = F(v)$ . When  $\mu = 0$ , the ion pitch angle

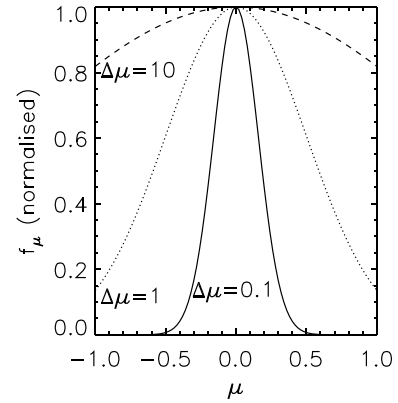


**Figure 2.** Illustrative  $f_{\mu}$  distributions for a range of widths  $\Delta\mu(v)$ : 0.1, 1, and 10. These three values correspond to  $v_n$  values 8.16, 0.86, and 0.23.

is perpendicular to the field line, and the angle-averaged case is recovered.

In this work, the use of the variable  $\mu$  in PION is algorithmically restricted to the calculation of  $F_{\mu}$  and  $D_{\text{RF}}$ . The returned distribution function is calculated internally as a function of both  $v$  and  $\mu$ , but then used as a function of  $v$  only. This ansatz does not account for poloidal variation of the distribution function, a refinement suitable for a future paper. Our purpose here is to study the effect of anisotropy on the effective  $D_{\text{RF}}$ .

The distribution width  $\Delta\mu(v)$  is calculated from the velocity distribution by equating expressions for the effective pitch angle  $\mu_{\text{eff}}^2(v)$ , a quantity that we define as the distribution-averaged  $\mu^2$ . We see by integration of its definition that this is equal to

$$\frac{\int_{-1}^1 \mu^2 F_{\mu}(v,\mu) d\mu}{\int_{-1}^1 F_{\mu}(v,\mu) d\mu} = \frac{[\Delta\mu(v)]^2}{2} - \frac{\Delta\mu(v)}{\sqrt{\pi}} \frac{e^{-\left(\frac{1}{\Delta\mu(v)}\right)^2}}{\operatorname{erf}\left(\frac{1}{\Delta\mu(v)}\right)}. \quad (8)$$

According to [35],  $\mu_{\text{eff}}^2(v)$  is also approximately equal to

$$\frac{1}{3} \frac{1 + v_n^2}{1 + v_n^2 + v_n^4}, \quad (9)$$

where  $v_n = 2v/v_{\gamma}$ ,  $v_{\gamma}$  being the characteristic velocity associated with pitch angle scattering [31]. Equating the expressions in equations (8) and (9) allows the numerical deduction of  $\Delta\mu(v)$ .

When  $v_n$  becomes large,  $\Delta\mu(v)$  becomes small, resulting in a narrow peak in  $f_{\mu}$ . Illustrative  $f_{\mu}$  distributions are shown in figure 2 for a spread of values of  $\Delta\mu(v)$ . In result, the population of particles becomes largely trapped at high energies.

### 3. Diffusion coefficient calculations

The crux of this work is the refinement of PION’s method for calculating the RF diffusion coefficient. PION has historically modelled this coefficient pitch angle averaged. To account



for the pitch angle variation, we begin from equation (10), the pitch angle averaged form for  $D_{\text{RF}}$ :

$$D_{\text{RF}}(v) = \sum_N K \int_{-1}^1 |E_+ J_{n-1}(k_{\perp} \rho) + E_- J_{n+1}(k_{\perp} \rho)|^2 d\mu. \quad (10)$$

Here  $K$  is a constant, and  $\rho = \frac{v}{\omega_{ci}} \sqrt{1 - \mu^2}$ , the ion Larmor radius. equation (10) is given in this form in [6]. It has a longer history, being given in a more general context in [25].

We improve on equation (10) by applying the ansatz given in equation (7) to weight the diffusion operator average according to the distribution in  $\mu$ , obtaining equation (11), the pitch angle resolved equation:

$$D_{\text{RF}}(v) = \sum_N K \int_{-1}^1 \left| \frac{F_{\mu}(v, \mu)}{F(v)} (E_+ J_{n-1}(k_{\perp} \rho) + E_- J_{n+1}(k_{\perp} \rho)) \right|^2 d\mu \quad (11)$$

where the ratio of distribution functions is taken from the assumed angular distribution given in equation (7). The effect is to weight the contribution to the equation by particle density according to the pitch angle. The former version of the calculation, in making an average over the angle, takes the intermediate functional form equation (10), equivalent to equation (11) with  $F_{\mu}(v, \mu) = F(v)$ . Equations (10) and (11) indicate that  $D_{\text{RF}}$  is influenced by the Bessel functions that capture FLR effects, generating  $v$ -space structure including minima in  $D_{\text{RF}}(v)$ . To calculate the angle-resolved distribution function used in equation (11), PION first calculates the 1D distribution function  $F(v)$ , and then converts this into a 2D  $v$ -space distribution  $F_{\mu}(v, \mu)$  using the Ansatz in equation (7).

In consequence of equations (10) and (11), energy plots of  $D_{\text{RF}}$  bear a strong resemblance to Bessel functions, with a near-zero minimum. The location and depth of these minima are critical in determining the quasi-linear term of the Fokker-Planck equation, and hence the rate at which the tail of the distribution function  $F$  drops off with  $v$ . We see that the angular distribution presented here has implications for the location of this minimum: the treatment of the angle smears the Bessel function argument  $k_{\perp} \rho$  across the range of values spanning from zero up to its value at  $\mu = 0$ . This alters both energy and RF diffusion coefficient minimum position values. Figure 3 shows characteristic curve shapes, produced with typical experimental parameters. The constant form (equation (1)), without angle treatment follows the form of its Bessel function inputs, with a series of zero minima, while the angle-averaged form (equation (10)) has only weak minima, at somewhat increased energy values. Resolving the angle (equation (11)) produces an intermediate case, due to the weighting in  $\mu$ .

Figure 4 compares the effect of averaging and resolving the pitch angle in this way for a pulse that will be considered in section 4. We see in this example a decrease in the first non-zero energy location of a  $D_{\text{RF}}$  minimum, from 2.47 to

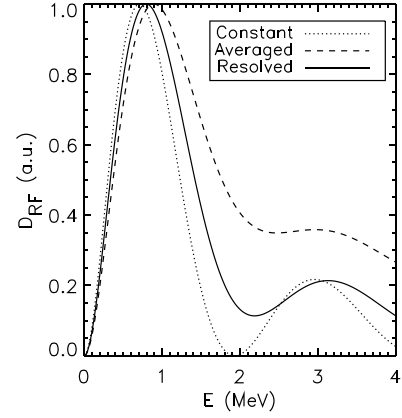


**Figure 3.** Typical variation of RF diffusion coefficient for the three formulations of the pitch angle. Parameters used: deuterium third harmonic,  $k_{\perp} = 56.6 \text{ m}^{-1}$ ,  $\frac{E_+}{E_-} = 0.43$ ,  $f_{\text{ICRH}} = 51.5 \text{ MHz}$ .

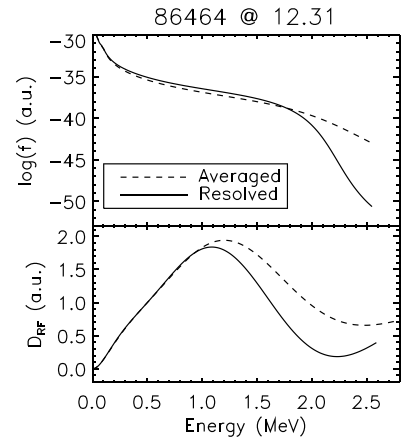


**Figure 4.** Variation of (above) distribution function  $F$ , and (below) RF diffusion coefficient for JET pulse 86464 at 12.31 s.

2.23 MeV, as well as a deeper minimum; the combination results in a markedly steeper tail to the distribution function, as we would expect.

Concluding this general analysis, we see several important variables between them determining the location of the diffusion coefficient first post-peak minimum. Both harmonic number and ion mass play key roles (as shown in figure 1 for the constant case, without angular dependence), the harmonic number in the orders of the Bessel functions, and the ion mass in the scaling of the energy axis. As the harmonic number increases, and as the ion mass decreases, the energy value of the first coefficient minimum reduces to experimentally measurable values. As is shown in section 4, the maximum energy value of the available experimental data does not exceed 2.3 MeV in any of the used cases. The upper limits are inherent to the used diagnostics, whose spectra are subject to documented experimental signal limitations [36, 37]. Two more parameters play key roles in determining  $D_{\text{RF}}$ . The perpendicular wavenumber  $k_{\perp}$  scales the arguments of the two Bessel functions, and the ratio of electric field polarisations  $E_+/E_-$  relatively weights the two Bessel functions against each other. The effects of these two parameters are important

in general to this calculation, but not in specific to the scope of this study.

The JET experimental database provides the input data needed to run PION for each pulse. This data is all time-evolving, and includes the equilibrium, the antenna wave frequency, minority concentrations, and plasma parameters. PION stores data for each pulse as a function of time points and normalised square root of poloidal flux surfaces. Simulations thus show the time evolution of absorption profiles and velocity distributions of resonant ions. The calculation of  $f$  and  $D_{RF}$  requires each of these parameters, with PION solving the coupled wave and Fokker-Planck equations in an iterative and self-consistent way.

## 4. Comparison for specific experiments

### 4.1. Second harmonic heating of hydrogen

As illustrated in figure 1, to find differences in  $D_{RF}$  and hence distribution function tail it is of advantage to look beyond the common fundamental heating scheme. For hydrogen plasma, we see these differences in second harmonic heating schemes. In demonstration, we consider a JET pulse studied in [11], 58738, which utilised this heating scheme as part of an experimental campaign studying the interactions of FLR effects with the high energy distribution tail. The heating of this pulse is hydrogen minority in deuterium. The position of the resonance is shown in figure 5.

We can compare PION's hydrogen distribution function with the output from the High Energy Neutral Particle Analyser [36], output which was for these pulses presented in [11]. Modelling pitch angle dependence to compute  $D_{RF}$  gives the expected clear improvement in simulation-to-experimental matching of the distribution tail for this case, as shown in figure 6.

The implemented pitch angle resolution has no significant effect on the heated ion species power partition for this case. We see only a small change in power partition with the pitch angle resolution. In this case, there is a 2.0% global increase, from 3.04 MW hydrogen absorption to 3.10 MW. Absorption by the majority and next strongest absorbing species, deuterium, is lower by five orders of magnitude. Locally, we see in the absorption profiles that weighting the distribution to trapped ions has resulted in a narrowing of the profile. We note that the electron absorption in this pulse is two orders of magnitude lower than the hydrogen absorption, barely visible in figure 10 for that reason.

### 4.2. Third harmonic heating of deuterium

For the case of third harmonic heating of deuterium, we re-examine JET pulses previously considered from a PION modelling perspective in [22, 23], 86459 and 86464. These pulses are from experiments dedicated to enhanced fusion production from deuterium-deuterium reactions [38]. Third harmonic heating of the deuterium population avoids both the heating of low energy particles found in fundamental heating and the interference of competing fundamental hydrogen heating

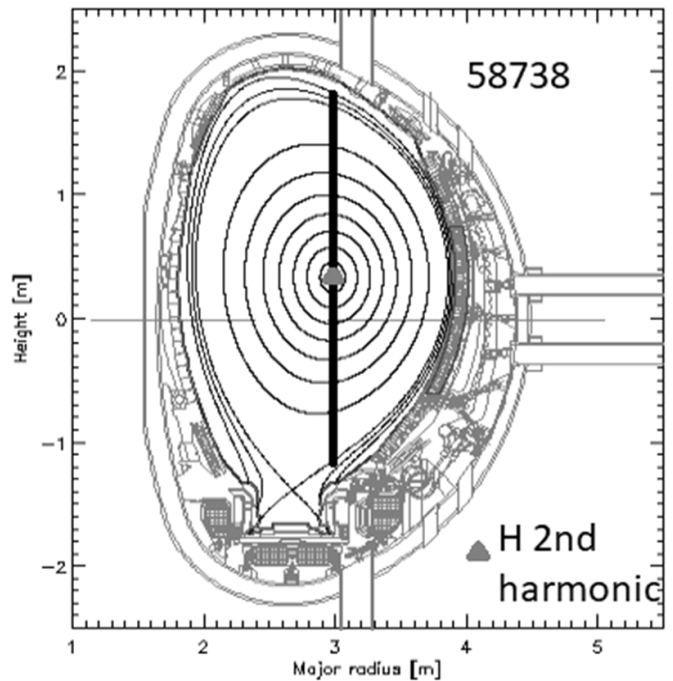


**Figure 5.** JET pulse 58738 at 23 s with the radial position of the heated hydrogen second harmonic overlaid.

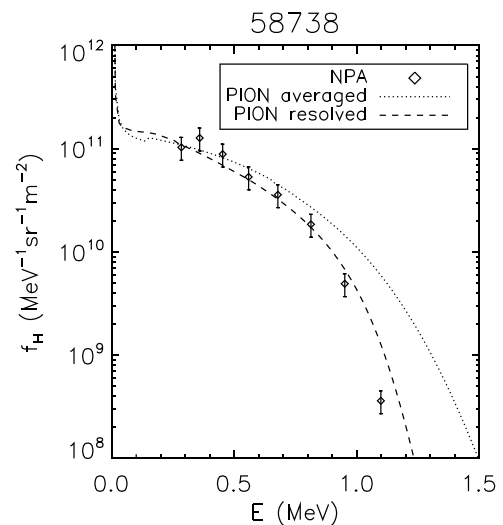


**Figure 6.** Hydrogen distribution functions  $F_H$  as given by PION without and with pitch angle resolution at  $t = 23$  s and the same as deduced from High Energy NPA measurements [36] (integrated in time from  $t = 22.5$  to  $23.5$  s) for JET discharge 58738 with second harmonic heating of hydrogen.

found in second harmonic deuterium heating. This scheme was used to create a population of deuterium ions in the MeV energy range to match the peak of the D-D reaction cross-section. This method produces a high energy tail to the deuterium distribution, precisely the condition of interest to this work. The position of the resonance for 86459 is shown in figure 7. The flux surface geometry and resonance position of 86464 are very similar to 86459, and are not shown.

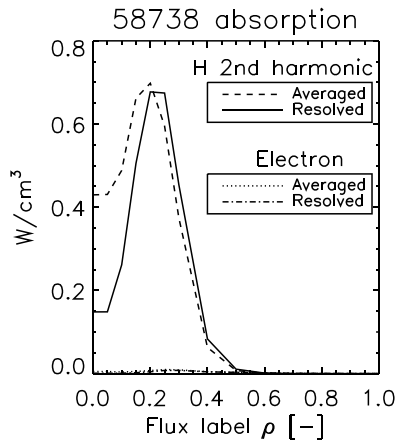


**Figure 7.** Heated ion species (hydrogen) and electron power absorption profiles for JET pulse 58738 at 23 s. Pitch angle averaged and resolved profiles are overlaid, as are the ion and electron profiles. The used flux label  $\rho$  is the square root of normalised poloidal magnetic flux.

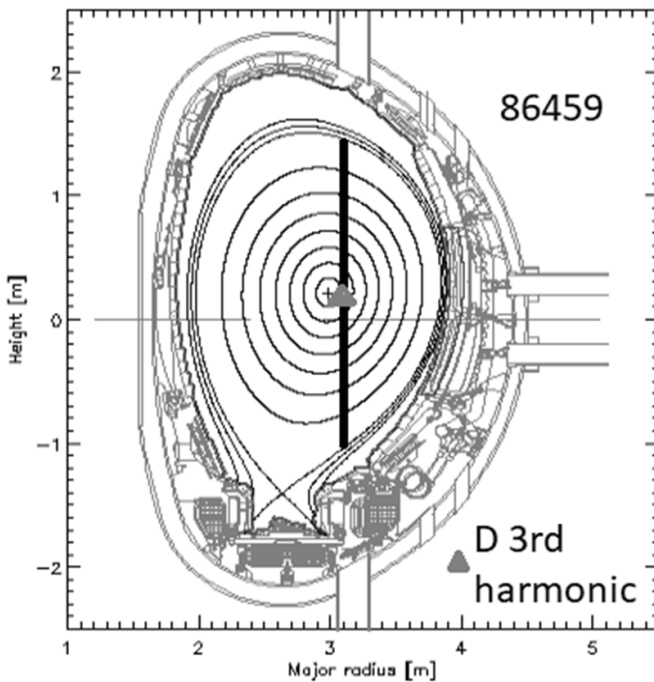


**Figure 8.** JET pulse 86459 at 12.31 s with the radial position of the heated deuterium third harmonic overlaid.

Figure 8(a) shows the spatially averaged energy distribution function as given by PION using both pitch angle averaged and pitch angle resolved ICRF diffusion coefficient calculations, comparing them with the experimental distribution functions for these discharges. The experimental values are those deduced from output of the 2.5 MeV TOFOR neutron spectrometer [37]. The TOFOR line of sight is vertical, and so it largely observes trapped populations, corresponding to  $\mu$  values close to zero.

Both models, averaged and resolved, are in good agreement with experimental results (within the error bars). The

**Table 1.** Power absorbed by deuterium as given by PION for 86459 and 86464.

86459	Power to D (MW)
Pitch angle averaged	1.41
Pitch angle resolved	1.77
86464	Power to D (MW)
Pitch angle averaged	1.35
Pitch angle resolved	2.05

distribution function is slightly stronger up to 1.5 MeV in the resolved case, which also explains the higher ion power absorption. Nevertheless, the difference becomes more relevant beyond 1.5 MeV, where the resolved distribution tail rapidly decreases as compared to the averaged tail, following the behaviour described by the RF diffusion coefficient in figure 4. The corresponding ICRF diffusion coefficients for the two angle-resolved cases are shown in figure 8(b). We note the locations of the diffusion coefficient minima in the regions of the strong decays in the distribution functions, as expected. We note also that in figure 8(a) we can see that the agreement in the low energy range, where pitch angle scattering becomes important, is less good. There are various candidate reasons for this, for example the low  $\nu$  pitch angle scattering resulting in  $f(\nu, \mu)$  being more independent of  $\mu$  at lower energy, departing from the assumption of equation (7) (compare figure 2). Other candidate reasons include simplifications used in the PION physical models and larger sensitivities in this energy range to uncertainties in the measured input data used in the modelling. The detailed investigation of these effects is beyond the scope of the present study, in which our focus is on the details of the high energy part of the distribution function. Nevertheless, we can see that PION is still able to also reproduce the measured trends in the low energy region; the PION distribution function for discharge 86459 always remains larger than that for discharge 86464, consistent with the measured trend.

The third harmonic deuterium heated pulses show a significant change in ion power absorption. The third harmonic deuterium scheme avoids overlap with hydrogen harmonics, and so there is no transfer of power between species. Rather, we see modelled enhancement to the deuterium heating, as shown in table 1. In the PION modelling of these pulses, we have included a parasitic damping effect as used in earlier modelling of the same discharges [23], where an assumed percentage of wave energy is damped at the plasma edge by other species. This technique is used because it has previously been demonstrated necessary for accurate PION power partition results for these third harmonic deuterium heating cases [39].

Considered globally, the changes in deuterium absorbed power shown in table 1 result from power previously parasitically absorbed now being absorbed by deuterium.



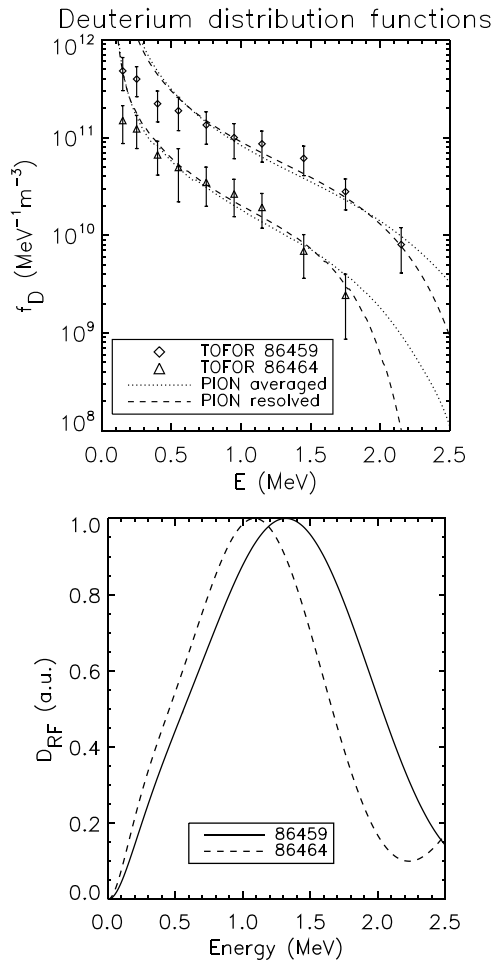


**Figure 9.** (a) Deuterium distribution function  $f_D$  as given by PION at  $t = 12.31$  s and the same as deduced from the TOFOR [37] measurements (diamonds and triangles; integrated in time from  $t = 11.5$  to  $12.5$  s) for JET discharges 86459 and 86464 at  $12.31$  s with third harmonic heating of deuterium and angular resolution of the RF diffusion coefficient; (b) RF diffusion coefficients for these two angle-resolved cases.

When we examine profile absorption for these two pulses at this time point (figure 9), we see a broadening of the deuterium absorption peak, which we may relate to the minor increase seen in figure 4 of the distribution function up to the point at which the tail drop-off starts, at  $1.5$ – $2$  MeV. We note that the electron absorption for these pulses is much stronger relative to the principal ion absorption than it is for the hydrogen second harmonic case studied in section 4.1, and is reduced when the pitch angle is resolved due to the increased ion absorption. The power deposition depends on the strength and polarisation of the wave field, as well as on the local absorption. The local absorption depends on the velocity distribution, which in turn depends on the power distribution, meaning that power depositions and particle distributions must be solved self-consistently. The parallel velocity distribution determines the Doppler broadening and thereby the radial width of the resonance layer. The difference between the scenarios of sections 4.1 and 4.2 is that the deuterium pulses have double the density of the hydrogen pulse, and also hotter

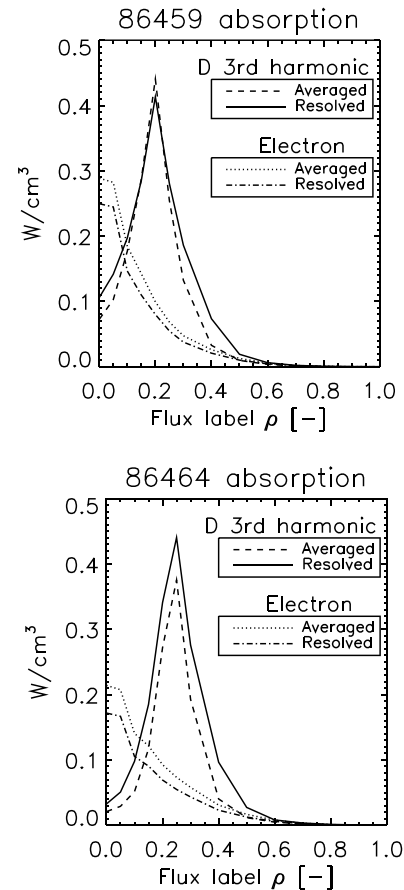


**Figure 10.** Heated ion species (deuterium) and electron power absorption profiles for JET pulses 86459 and 86464 at  $12.31$  s. Pitch angle averaged and resolved profiles are overlaid, as are the ion and electron profiles. The used flux label  $\rho$  is the square root of normalised poloidal magnetic flux.

electrons. The combination creates substantial electron damping, seen in figure 9, but not seen in figure 10.

## 5. Conclusions

A refinement to the modelling of the RF diffusion operator in the PION code has been implemented and its results compared for JET cases where the changes were expected to be of significance. This refinement consists of including a physics-based Ansatz for the fast ion distribution function dependence on pitch angle, instead of an averaging process assuming this is uniform. We have observed improved agreement between the modelled distribution function and measurements in the high energy tail in hydrogen and deuterium plasmas with higher harmonic heating schemes. We have also observed changes to the power absorption as a result of this modification.

While offering improved analysis of existing pulses in the JET data library, this refinement also has relevance to analyses on future devices. For example, among the current ITER scenarios, there are three that utilise second harmonic hydrogen heating, labelled T.a, T.b, and T.c; these are the so-called ‘third-field’ cases, labelled ‘T’ because  $B_0$  is one third of the full available ITER  $B_0$ . These have been analysed with PION

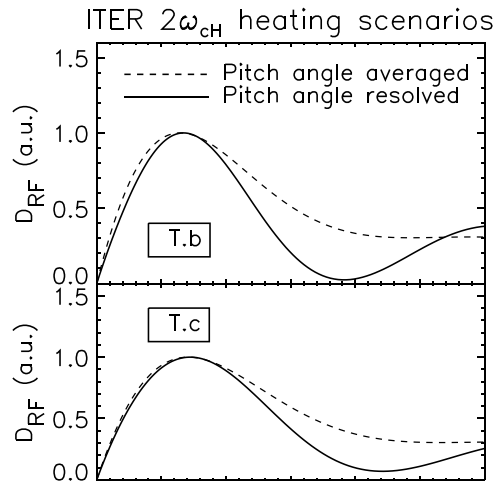


**Figure 11.** RF diffusion coefficients for selected second harmonic hydrogen heating ITER scenarios T.b (above) and T.c (below) calculated with pitch angle averaged and pitch angle resolved.

in [21], in which parameters are given that are sufficient for the calculation of generic diffusion coefficient energy profiles for these scenarios, as in figure 3.

On producing these profiles in pitch angle resolved form, we see that cases T.b and T.c both exhibit diffusion coefficient minima in the low MeV range, as shown in figure 11. We also see in comparing the pitch angle averaged and resolved versions of  $D_{RF}$  that the minimum is much less present in the averaged version, especially for T.b. This is precisely the behaviour that makes the angular dependence as documented in this paper important in calculating the distribution tail. This modelling refinement will be important for these scenarios, and the planned gamma-ray diagnostics for ITER [40, 41] will provide experimental data to verify against.

The results presented above illustrate the difficulty in predicting consistent effects of this model alteration on global quantities. The non-linear nature of ICRF physics interacts with the change in complex ways. The subject of power partitioning, addressed above for each experiment, shows the possible variation in outputs, with variable increases in the power absorbed by the resonant ion species, covering the range 2%–51% in the three JET pulses described in this paper. There are a number of phenomena that affect these outputs. Firstly, there are multiple possible absorptions—in addition to the specific species absorption targeted in a given pulse, other species may also see significant resonances. There may be parasitic resonances, as included in this modelling for 86459 and 86464. There will also be direct electron absorption. Having observed this for JET data, and noted that similarly relevant experimental regimes are planned for ITER operation, it is to be expected that the impacts of including these effects will be similar on ITER.

### Data availability statement

The data generated and/or analysed during the current study are not publicly available for legal/ethical reasons but

are available from the corresponding author on reasonable request.

### Acknowledgments

The CCFE part of this work has been carried out within the framework of the EUROfusion Consortium and has received funding from the Euratom research and training programme 2014–2018 and 2019–2020 under Grant Agreement No. 633053. The views and opinions expressed herein do not necessarily reflect those of the European Commission.

The BSC part of this project is co-financed by the European Union Regional Development Fund within the framework of the ERDF Operational Program of Catalonia 2014–2020 with a grant of 50% of total cost eligible.

The authors are grateful to Jacob Eriksson for assistance with experimental data, to Lars-Göran Eriksson for discussions on the implementation of the new features, and to Colin Roach and Michael Fitzgerald for valuable comments on the manuscript.

### ORCID iDs

D M A Taylor  <https://orcid.org/0000-0002-0465-2466>

D Gallart  <https://orcid.org/0000-0003-1663-3550>

### References

- [1] Ongena J *et al* 2017 *Plasma Phys. Control. Fusion* **59** 054002
- [2] Wilson J R and Bonoli P T 2015 *Phys. Plasmas* **22** 021801
- [3] Noterdaeme J-M 2020 *AIP Conf. Proc.* **2254** 020001
- [4] Eriksson L-G and Hellsten T 1995 *Phys. Scr.* **52** 70–79
- [5] Eriksson L-G, Hellsten T and Willén U 1993 *Nucl. Fusion* **33** 1037
- [6] Mantsinen M J 1999 *Development and Experimental Evaluation of Theoretical Models for Ion Cyclotron Resonance Frequency Heating of Tokamak Plasmas* (Helsinki University of Technology)
- [7] Start D F H *et al* 1998 *Phys. Rev. Lett.* **80** 4681
- [8] Start D F H *et al* 1999 *Nucl. Fusion* **39** 321
- [9] Garcia J, Challis C, Gallart D, Garzotti L, Görler T, King D and Mantsinen M 2017 *Plasma Phys. Control. Fusion* **59** 014023
- [10] Mantsinen M J *et al* 2002 *Phys. Rev. Lett.* **88** 105002
- [11] Salmi A *et al* 2006 *Plasma Phys. Control. Fusion* **48** 717
- [12] Mantsinen M J, Jarvis O N, Kiptily V G, Sharapov S E, Alper B, Eriksson L-G, Gondhalekar A, Heeter R F and McDonald D C 2001 *Nucl. Fusion* **41** 1815
- [13] Gallart D *et al* 2018 *Nucl. Fusion* **58** 106037
- [14] Mantsinen M J *et al* 2015 *AIP Conf. Proc.* **1689** 030005
- [15] Mantsinen M J *et al* 2016 *43rd EPS Conf. on Plasma Physics* vol 40A
- [16] García-Muñoz M, Fahrbach H-U, Günter S, Igochine V, Mantsinen M J, Maraschek M, Martin P, Piovesan P, Sassenberg K and Zohm H 2008 *Phys. Rev. Lett.* **100** 055005
- [17] Sharapov S E *et al* 2017 *Plasma Phys. Control. Fusion* **60** 014026
- [18] Mantsinen M J, Petty C C, Eriksson L-G, Mau T K, Pinsker R I and Porkolab M 2002 *Phys. Plasmas* **9** 1318
- [19] Eriksson L-G *et al* 2017 *Phys. Plasmas* **24** 022122

- [20] Becoulet A *et al* 2000 *J. Plasma Fusion Res.* **3** 51–57  
(available at: [www.jspf.or.jp/JPFERS/PDF/Vol3/jpfrs2000\\_03-051.pdf](http://www.jspf.or.jp/JPFERS/PDF/Vol3/jpfrs2000_03-051.pdf))
- [21] Arbina I L *et al* 2019 *Proc. 46th EPS Conf. Plasma Physics* vol P4 p 1079
- [22] Schneider M *et al* 2016 *Nucl. Fusion* **56** 112022
- [23] Mantsinen M J *et al* 2015 *IAEA Technical Meeting n Energetic Particles (Vienna)* (available at: [www.naweb.iaea.org/napc/physics/meetings/TM49508/website/Papers/Mantsinen%20M.pdf](http://www.naweb.iaea.org/napc/physics/meetings/TM49508/website/Papers/Mantsinen%20M.pdf))
- [24] Budny R V *et al* 2012 *Nucl. Fusion* **52** 023023
- [25] Kennel C F and Engelmann F 1966 *Phys. Fluids* **9** 2377
- [26] Eriksson L-G and Helander P 1994 *Phys. Plasmas* **1** 308
- [27] Llobet X *et al* 1988 *Theory of Fusion Plasmas (Proc. Joint Varenna-Lausanne Int. Workshop, Chexbres)* (Bologna: Editrice Compositori) p 663
- [28] Villard L, Appert K, Gruber R and Vaclavik J 1996 *Comput. Phys. Rep.* **4** 95
- [29] Budden K G 1961 *Radio Waves in the Ionosphere* (Cambridge: Cambridge University Press)
- [30] Eriksson L-G *et al* 1999 *Phys. Rev. Lett.* **81** 1231
- [31] Stix T H 1972 *Plasma Phys.* **14** 367
- [32] Anderson D, Core W, Eriksson L-G, Hamnén H, Hellsten T and Lisak M 1987 *Nucl. Fusion* **27** 911
- [33] Stix T H 1992 *Waves in Plasmas* (American Institute of Physics)
- [34] McClements K G 1987 *Sol. Phys.* **109** 355
- [35] Anderson D, Eriksson L G and Lisak M 1987 *Plasma Phys. Control. Fusion* **29** 891
- [36] Korotkov A A, Gondhalekar A and Stuart A J 1997 *Nucl. Fusion* **37** 35
- [37] Gatu Johnson M *et al* 2008 *Nucl. Instrum. Methods A* **591** 417
- [38] Sharapov S E *et al* 2016 *Nucl. Fusion* **56** 112021
- [39] Eriksson L-G, Mantsinen M J, Rimini F G, Nguyen F, Gormezano C, Start D F H and Gondhalekar A 1998 *Nucl. Fusion* **38** 265
- [40] Kiptily V G, Cecil F E and Medley S S 2006 *Plasma Phys. Control. Fusion* **48** R59
- [41] Chugunov I N, Shevelev A E, Gin D B, Kiptily V G, Gorini G, Nocente M, Tardocchi M, Doinikov D N, Naidenov V O and Khilkevitch E M 2011 *Nucl. Fusion* **51** 083010